How to Cite: Dzeranov, A.A., Bondarenko, L.S., Prokofiev, M.V., Bondarenko, R.A., Abramov, D.R., Dzhardimalieva, G.I. & Kydralieva, K.A. (2026). Size and Magnetization Control of Magnetite NPs via Ethylene Glycol and Temperature for Ferrofluid and Magnetotargeting: Model Experiments. *Eurasian Journal of Chemistry, 31, 1(121), 137–150.* https://doi.org/10.31489/2959-0663/1-26-10

Article

Received: 11 December 2025 | Revised: 27 February 2026 | Accepted: 2 March 2026 | Published online: 19 March 2026

UDC 544.42+519.242.7

https://doi.org/10.31489/2959-0663/1-26-10

Artur A. Dzeranov[1, 2*], Lyubov S. Bondarenko[1], Michail V. Prokofiev[1], Roman A. Bondarenko[3], Danil R. Abramov[1], Gulzhian I. Dzhardimalieva[1, 2], Kamila A. Kydralieva[1]

[1]*Moscow Aviation Institute (National Research University), Moscow, Russia;*
[2]*Federal Research Center of Problems of Chemical Physics and Medicinal Chemistry, Chernogolovka, Russia;*
[3]*Institute of Applied Mechanics, Russian Academy of Sciences, Moscow, Russia*
*(*Corresponding author's e-mail: arturdzeranov99@gmail.com)*

Size and Magnetization Control of Magnetite NPs via Ethylene Glycol and Temperature for Ferrofluid and Magnetotargeting: Model Experiments

Magnetic nanoparticles (NPs) are highly promising materials for diverse biomedical applications, particularly in magnetotargeting, owing to their tunable magnetic properties. Achieving precise control over their synthesis parameters is critical for optimizing these properties and ensuring their efficacy. This study investigates the impact of synthesis conditions on the properties of magnetite (Fe_3O_4) nanoparticles. A set of magnetite NPs were prepared via co-precipitation of ferrous and ferric ions by a base in ambient conditions, systematically varying the ratio of ethylene glycol/water (EG/water) solvents and temperatures (4, 20, and 70 °C). Crystal structure, morphology and magnetic parameters were analyzed. Additionally, rheological experiments were conducted to study the dynamic viscosity of ferrofluids containing varying sizes and concentrations NPs in polyglucinum. Results showed that Fe_3O_4 NPs size linearly increased with the EG/water volume ratio only at 70 °C. Increasing EG from 0 % to 50 % elevated magnetite stoichiometry from $Fe_{2.72}O_4$ to $Fe_{2.912}O_4$ with higher concentrations reducing it. The effect of temperature on stoichiometry varied depending on the ethylene glycol (EG) content. At low EG content, stoichiometry decreased with increasing temperature. But, at higher EG content, maximum stoichiometry was observed at 20 °C. Increasing polydispersity of NPs (0.07–0.13) decreased viscosity in polyglucinum from ~10 to ~4 mPa s (1–5 % EG). Evaluation tests of the magnetic induction gradient on NPs capture in a flow-through setup were also performed. A sigmoidal relationship ($R^2 = 0.97$) was established between the NPs capture efficiency and the magnetic induction gradient. These findings provide valuable insights for optimizing the synthesis and suspension performance for magnetic fluids for magnetotargeting applications.

Keywords: Synthesis of magnetic NPs, Ethylene glycol, Synthesis temperature, Oxidation, Size control, Saturation magnetization, Rheology, Magnetic capture

Introduction

Magnetite (Fe_3O_4) is among the most extensively studied magnetic NPs due to its unique combination of various properties making it highly attractive for numerous biomedical applications, such as magnetic resonance imaging [1], drug/gene delivery [2–5], in catalysis [6–8], in ferroptosis therapy due to Fe^{2+}/Fe^{3+} mediators of Fenton and Fenton-like reactions [9–11] as well as ferrofluids [12]. Uniformity of magnetite NPs size, shape, and crystalline structure is crucial in biomedical applications [13] that require the design and synthesis of NPs with the perfectly controlled features such as magnetization of NPs. The latter is a size dependent property, so, it can utilize its size-in dependent version that is called saturation magnetization (σ_s) [14]. Many reports of solution-phase synthesis of monodisperse magnetite nanocrystals (MNCs) have been published [15–17]. However, lack of reproducibility of MNC synthesis is a persistent problem, and the keys to producing monodisperse MNCs remain elusive [18]. The structural characteristics and subsequently magnetic properties of materials are greatly originated from their synthesis process [19–23]. In recent studies of coprecipitation synthesis, there have been many reports on changing various experimental parameters to control the size of Fe_3O_4 NPs, such as altering the reaction temperature and reaction time in synthesis [24, 25], varying the Fe^{2+}/Fe^{3+} cation ratio, and pH [26], stirring velocity [27], etc. Interfacial tension of the medium is also expected to be one factor in controlling the size NPs. Ethylene glycol (EG) is a solvent miscible with water at any composition [28]. Besides, EG have a high boiling point (246 °C) and a

low interfacial tension (47.99 mN m^{-1}) [29]. It can be therefore expected that EG becomes a useful additive for controlling the size of magnetite produced by a forced hydrolysis reaction at an elevated temperature. Moreover, EG being a polyol capable of acting as a reducing and stabilizing agent, influencing stoichiometry of magnetite as well as nucleation and growth processes. Recent mechanistic work also shows that, in alcohol-based systems, the water fraction and oxygen access can be decisive for iron nanoparticle oxidation pathways and kinetics, underscoring why solvent composition must be treated as a primary control parameter [30]. This paper demonstrates a synthesis of magnetite NPs via co-precipitation of ferrous and ferric ions by a base in ambient conditions of 10 to 34 nm in diameter regulated by changing the ratio of EG/water and temperature from 4 to 70 °C. We investigated in this paper the influence of both EG and temperature on the size, polydispersity, stoichiometry and saturation magnetization (σ_s) of NPs. Selected NPs samples were tested under model conditions to assess their effect on the dynamic viscosity of polyglucinum-based ferrofluids, as well as the influence of magnet induction on NPs capture in a model flow-through setup.

Experimental

Preparation of Fe_3O_4 NPs

Magnetite NPs Fe_3O_4 with different sizes were synthesized using the co-precipitation method by Elmore reaction [31] by changing the volume ratio of ethylene glycol/water (EG/water) and temperature while keeping the other experimental conditions the same. 150 mL of a 0.05 M $FeSO_4 \cdot 7H_2O$ and 0.1 M $FeCl_3 \cdot 6H_2O$ solution was poured in a beaker in ambient (air) conditions for technological reason and the solution's temperature was maintained at 4, 20 or 70 °C. 1 M NaOH was added dropwise into the solution in order to reach pH 9 and stirred at 300 rpm for 30 min. pH control was over time. The product was harvested by magnetic separation, washed repeatedly with deionized water 3 times with a hydromodulus of 1:50 and then dried at 70 °C. Storage conditions were in a sealed container in a dark place. Synthesis conditions and cipher of NPs are presented in Table 1.

Table 1

Synthesis conditions and cipher of NPs

T, °C	EG, volume ratio			
	0	25	50	75
4	4/0*	4/25	4/50	4/75
20	20/0	20/25	20/50	20/75
70	70/0	70/25	70/50	70/75
*the code in the name of the samples indicates the temperature (first index) and the volumetric content of EG.				

Characterization of NPs

NPs samples were characterized using X-ray diffraction (XRD) analysis, transmission electron microscopy (TEM), and vibrating sample magnetometer (VSM) analysis. Method descriptions are provided in Supporting Information (SI).

Results and Discussion

The Influence of Ethylene Glycol Concentration and Temperature on the Morphology of NPs

The TEM images taken to determine the morphology, shape and size distribution for the selected NPs produced at the different volume ratios EG/water and temperature are shown in Figure 1. The resulting magnetite nanoparticle samples are found to be nearly of spherical/cubic shape. For samples 4/25, 20/25 and 70/25, the average particle size was 16.7, 19.1 and 14.1 nm, respectively; for samples 70/0, 70/50 and 70/75, it was 9.8, 22.6 and 33.6 nm, respectively. The size particle distribution histograms constructed from TEM images show that with increasing EG in the synthesized solution, the range of particle sizes increases. The electron diffraction patterns in the selected region obtained by TEM are shown in Figure S1 (SI). The ring diameters of the corresponding atomic planes indicate that the main phase of the NPs is magnetite [AMCSD 0002400, Supplementary Materials].

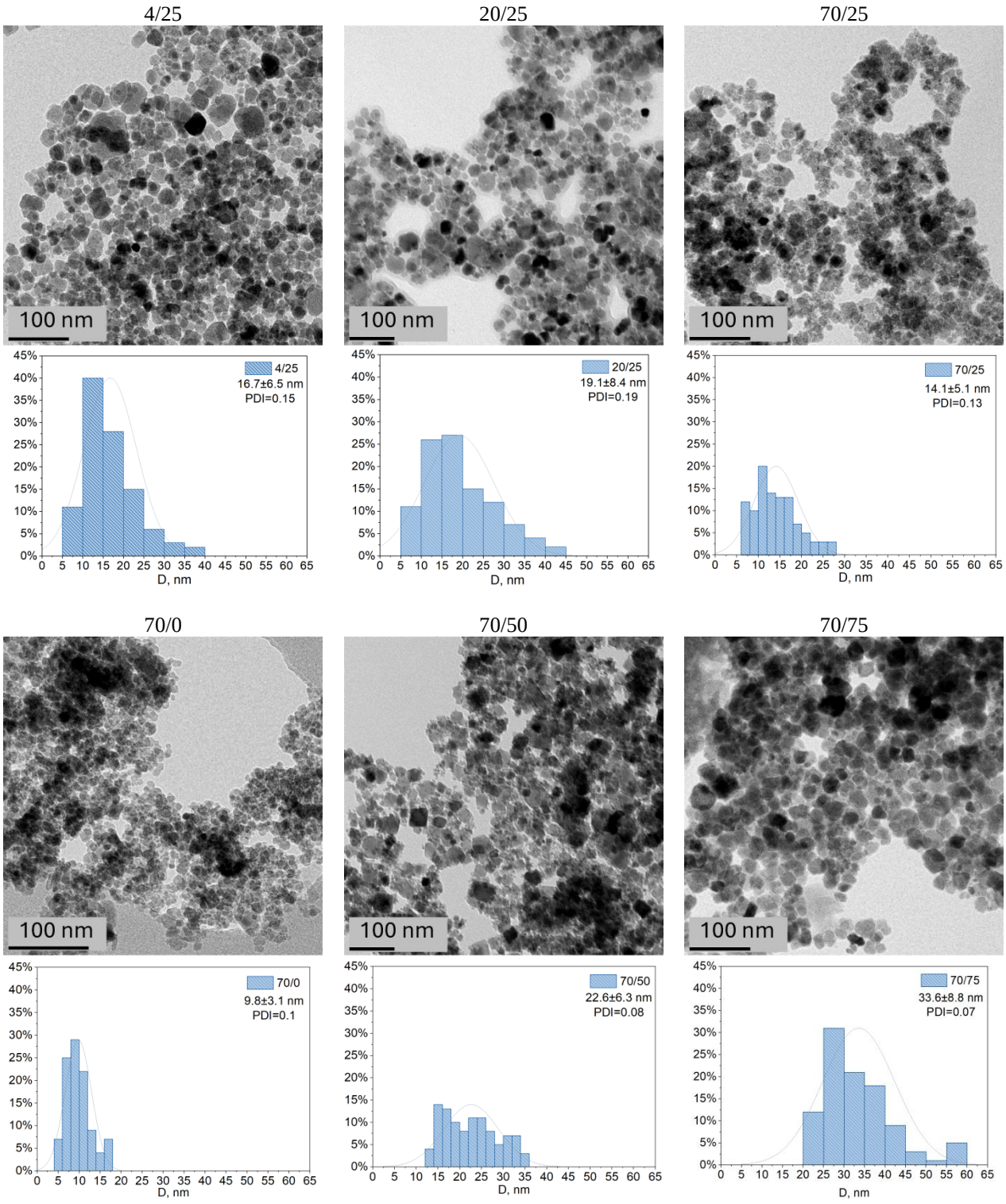

Figure 1. TEM images and plotted particle size distribution histograms

For these samples, graphs were constructed showing the dependence of NPs size on the EG content in the solution and the synthesis temperature. The results are presented in Figure 1*a*, *b*.

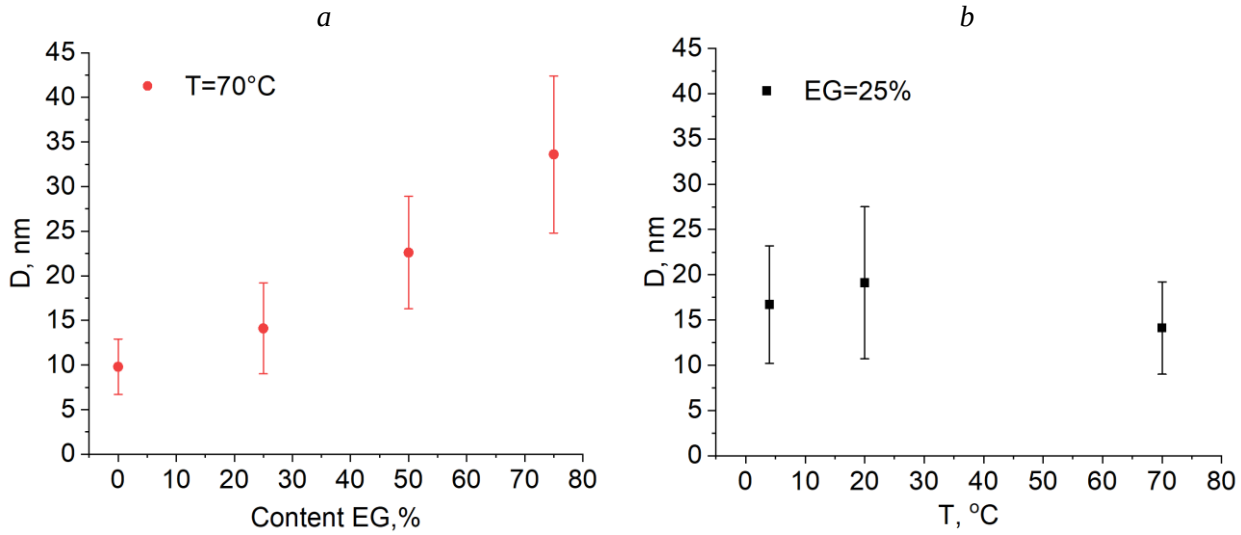

Figure 2. Dependence of NPs size on the EG content (*a*) and the synthesis temperature (*b*)

Although size distribution NPs with irregular shapes (Fig. 1) could be found due to the inevitable fluctuations in a coprecipitation system, the trend that the size and shape of the NPs controlled by the synthesis conditions was obvious. Figure 2*a* shows that with increasing EG content, the particle size increases, which is due to an increase in the viscosity of the solution, since the density of EG is higher than the density of water, and the density of the solution increases with increasing EG concentration (from 0.41 to 2.3 mPa s for water and 75 % EG, respectively, at 70 °C). A statistically significant difference exists only between samples 70/0 and 70/75, p-value = 0.009. Xu et al. found that anisotropic octahedral Fe_3O_4 NPs vary the particle sizes from 30 to 115 nm by changing the volume ratios of ethylene glycol/diethylene glycol in hydrothermal synthesis [32].

Temperature can play a crucial role in the phase formation in process, e.g. due to the increased loss of ammonia (in case of NH_4^+ present in the system) with increased temperature and its implications for the phase formation kinetics [33]. According to [33] in aqueous solution, synthesis at the lowest temperature of 5 °C exhibit magnetite phase, while increase in the growth temperature to 95 °C leads to pure maghemite phase. Authors noted that since the temperatures used here are too small for solid state transformations, the observed changes should occur primarily in the particle formation process itself where the role of precursor radicals can be temperature sensitive. Moreover, the grains in the case of the 27 °C sample are much smaller (6–8 nm), in the case of the 95 °C sample, the grains are somewhat bigger than the 27 °C case and they are again better faceted though smaller than the 5 °C case. But, in our experiments no dependence of NPs size is observed on the temperature of EG-assisted synthesis. The above phenomena about the influence of temperature on the size of Fe_3O_4 particle can be interpreted by thermophysical properties of EG: heat capacity and thermal conductivity decrease (compared to water) by up to 20 % with increasing EG concentration and decreasing operating temperatures in the low zone; kinematic and dynamic viscosity are 2-3 times higher than that of water at positive temperatures and increase by 8–10 times as the concentration increases to the practical limit of 65 %.

X-Ray Diffraction Analysis

The phase composition of magnetic NPs was also investigated by XRD (Fig. 13). A typical diffraction pattern was observed, confirming the presence of the magnetite phase (Fe_3O_4). The content of magnetite and maghemite was calculated using the Rietveld method (Fig. 3). The obtained unit cell parameter values for all samples were smaller than those of magnetite (8.396–8.400 Å according to ICDD-PDF 19–629), but larger than those of maghemite (8.33–8.34 Å according to ICDD-PDF 39–1346). This is explained by partial oxidation of Fe^{2+} ions during drying and/or storage and modification, leading to the formation of non-stoichiometric magnetite with the formula $Fe_{3-\delta}O_4$, where δ can vary from zero (stoichiometric magnetite) to 1/3 (fully oxidized).

4/0

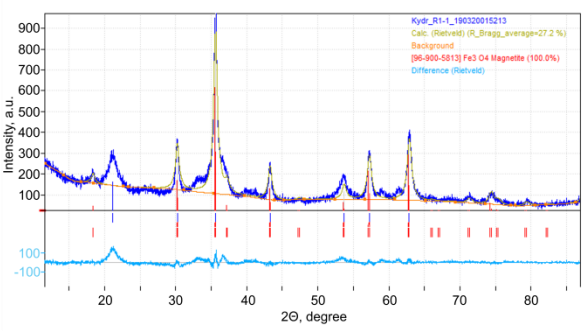

4/25

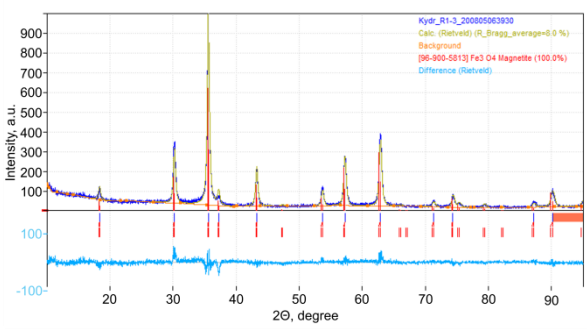

4/50

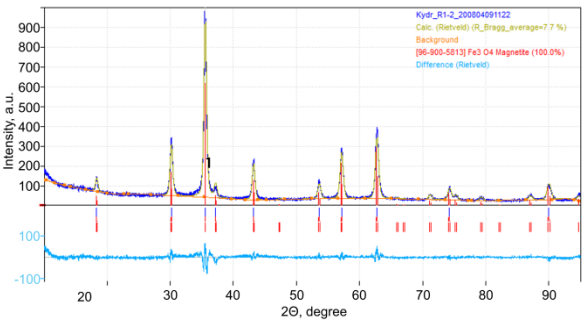

4/75

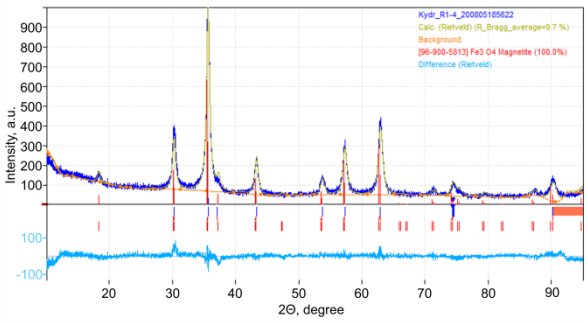

20/0

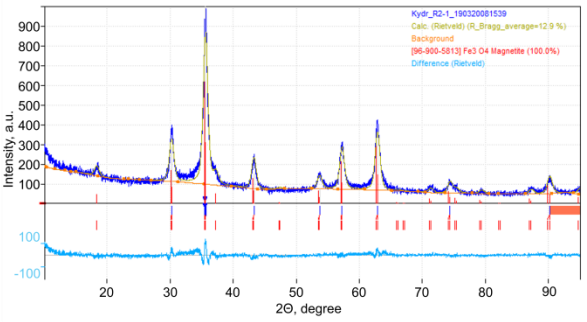

20/25

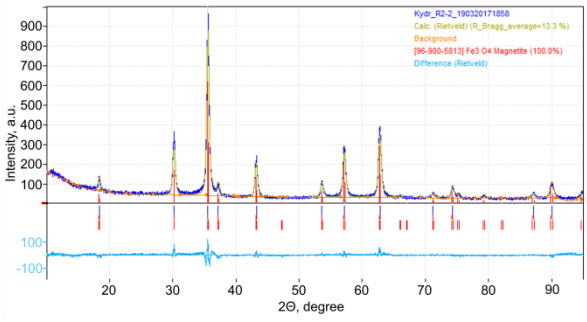

20/50

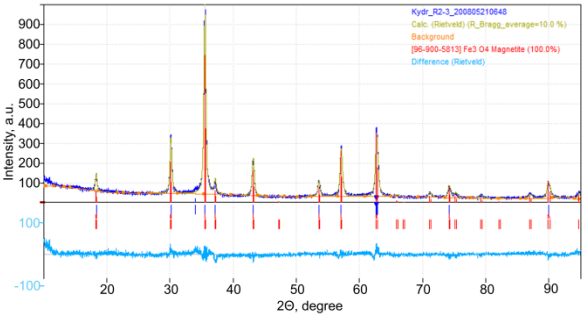

20/75

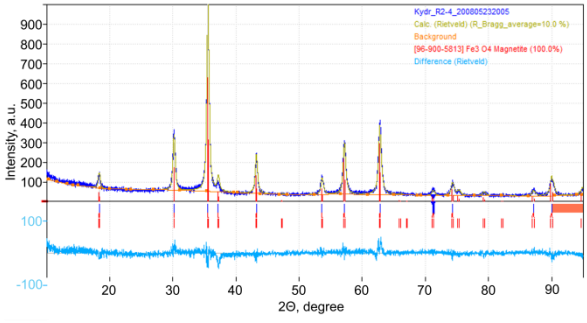

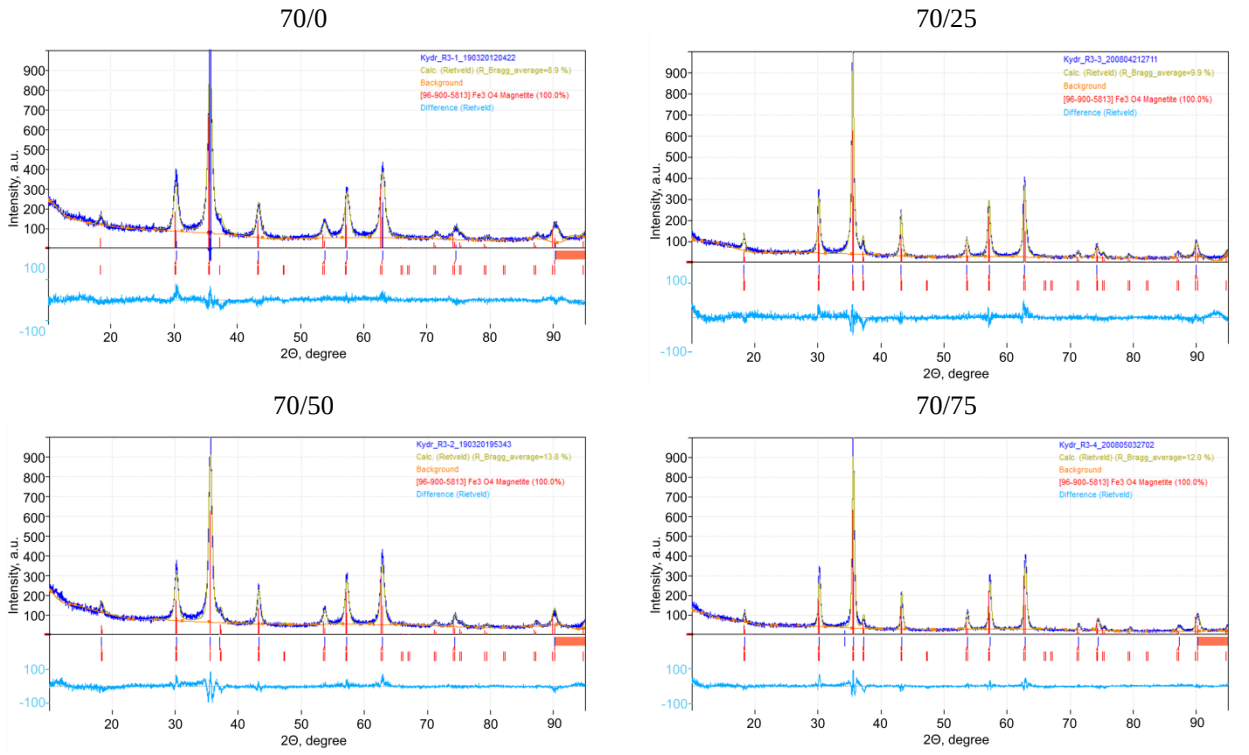

Figure 3. Diffraction patterns of NPs

The calculated stoichiometric formulas of magnetite samples and crystallite sizes calculated using the Williamson-Hall method [34] are presented in Table 2.

Table 2

Formula and crystallite size of iron oxide NPs

Sample	*a*, Å	$(GoF)^2$	Composition	Amount, %	*D*, nm	No. COD
4/0	8.363	0.7	$Fe_{2.83}O_4$	88.1	8.40	9005838
4/25	8.374	1.1	$Fe_{2.90}O_4$	96.1	22.20	9005838
4/50	8.358	1.6	$Fe_{2.80}O_4$	92.6	29.00	9005838
4/75	8.354	0.9	$Fe_{2.77}O_4$	96.2	18.40	9005838
20/0	8.361	0.8	$Fe_{2.82}O_4$	96.4	12.50	9007706
20/25	8.373	0.8	$Fe_{2.89}O_4$	96.5	26.00	9005839
20/50	8.378	1.0	$Fe_{2.912}O_4$	96.5	31.50	2101926
20/75	8.368	1.1	$Fe_{2.86}O_4$	96.4	24.40	9005839
70/0	8.345	1.0	$Fe_{2.72}O_4$	96.2	11.80	9002319
70/25	8.359	0.9	$Fe_{2.81}O_4$	96.5	20.80	9005842
70/50	8.376	0.6	$Fe_{2.91}O_4$	96.1	27.90	2101926
70/75	8.357	0.6	$Fe_{2.79}O_4$	95.9	28.20	9005839

The average size of NPs for the 70/0, 70/25, 70/50 and 70/75 samples are close to the results obtained using TEM. According to X-ray diffraction data, the presence of EG in the reaction mixture, compared to temperature and solution viscosity, is the most significant factor influencing crystallite size (Fig. 4*a*). The maximum magnetite content and its most stoichiometric form (with a 3-δ parameter in the range of 2.89–2.91) were observed at a solution viscosity of 1.3–4.5 mPa s and an EG content of 25–50 % (Fig. 4*b*). This confirms the active participation of EG in the reduction of iron (III) salts in an alkaline medium. A further increase in the EG concentration to 70 % and the observed decrease in the stoichiometry of magnetite are associated with a decrease in the equivalent water content in the system required for coprecipitation methods where the hydrolysis of ferrous and ferric ions, ferrous hydroxide ($Fe(OH)_2$) and goethite

(-FeOOH), are coprecipitated as precursors in an alkaline solution according to Elmore reaction. For the samples synthesized at 20 and 70 °C, the peak stoichiometry was achieved at a content of 50 % EG and amounted to $Fe_{2.912}O_4$ and $Fe_{2.91}O_4$, respectively, while at 4 °C the peak stoichiometry was achieved at a content of 25 % EG and amounted to $Fe_{2.9}O_4$ (i.e. mixture 60 % magnetite and 31 % maghemite) [35]. Our previous studies showed that a change in the stoichiometry of magnetite, associated with the partial transformation to maghemite phase, leads to a change in the biological activity of NPs compared to stoichiometric magnetite [36, 37].

The stoichiometry of magnetite is important and essential parameter because the Fe^{3+}/Fe^{2+} ions pair mediates Fenton oxidation-reduction reactions, which are the primary mechanism triggering ferroptosis [38]. The magnetite stoichiometry in samples prepared at volume ratios of 0/100 and 25/75 (EG/water) steadily decreases with increasing synthesis temperature, likely due to the oxidation of iron ions. In contrast, samples prepared at 50/50 and 75/25 (EG/water) exhibited a peak at 20 °C of coprecipitation conditions followed by decline. This behavior is explained by the fact that, at this temperature, the reducing potential of EG outweighs the oxidizing effect of increasing temperature.

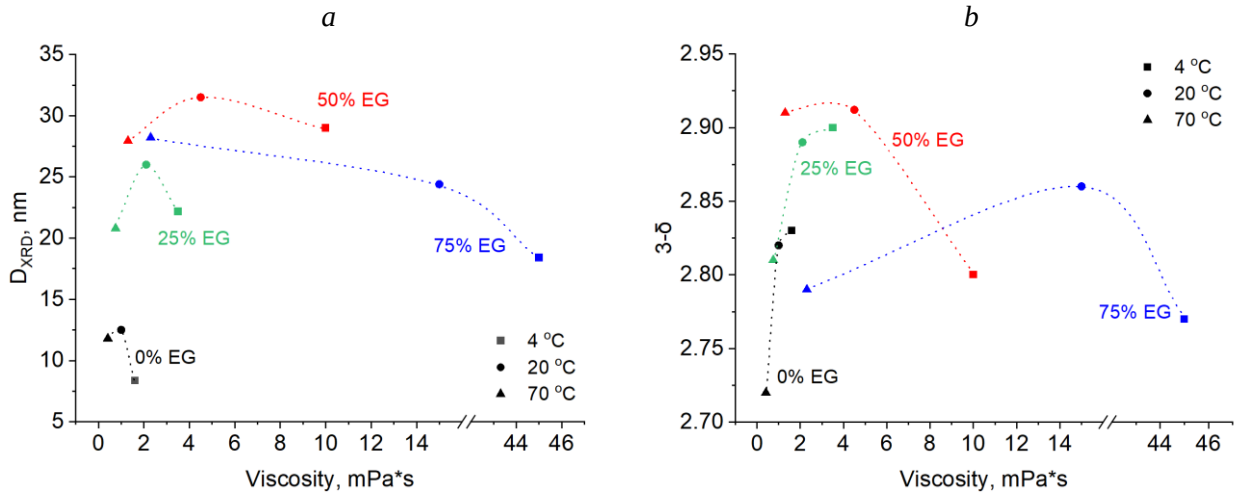

Figure 4. Dependence of crystallite size (*a*) and magnetite stoichiometry (*b*) on solution viscosity and synthesis temperature

The optimal EG content facilitates controlled synthesis due to two factors: firstly, as a reducing agent, it determines the kinetics of magnetite nucleation; secondly, by modifying the viscosity of the medium, it influences the diffusion coefficient of the reactants, slowing the growth rate and promoting the formation of larger, more perfect crystals with a minimum of defects.

Magnetic Properties of Magnetite NPs

The results of the analysis of the magnetic properties of magnetite are presented as hysteresis loops (Fig. 5). Table 3 presents the values of saturation magnetization (σ_s), remanent magnetization (σ_r), and coercivity (H_c) for magnetite NPs.

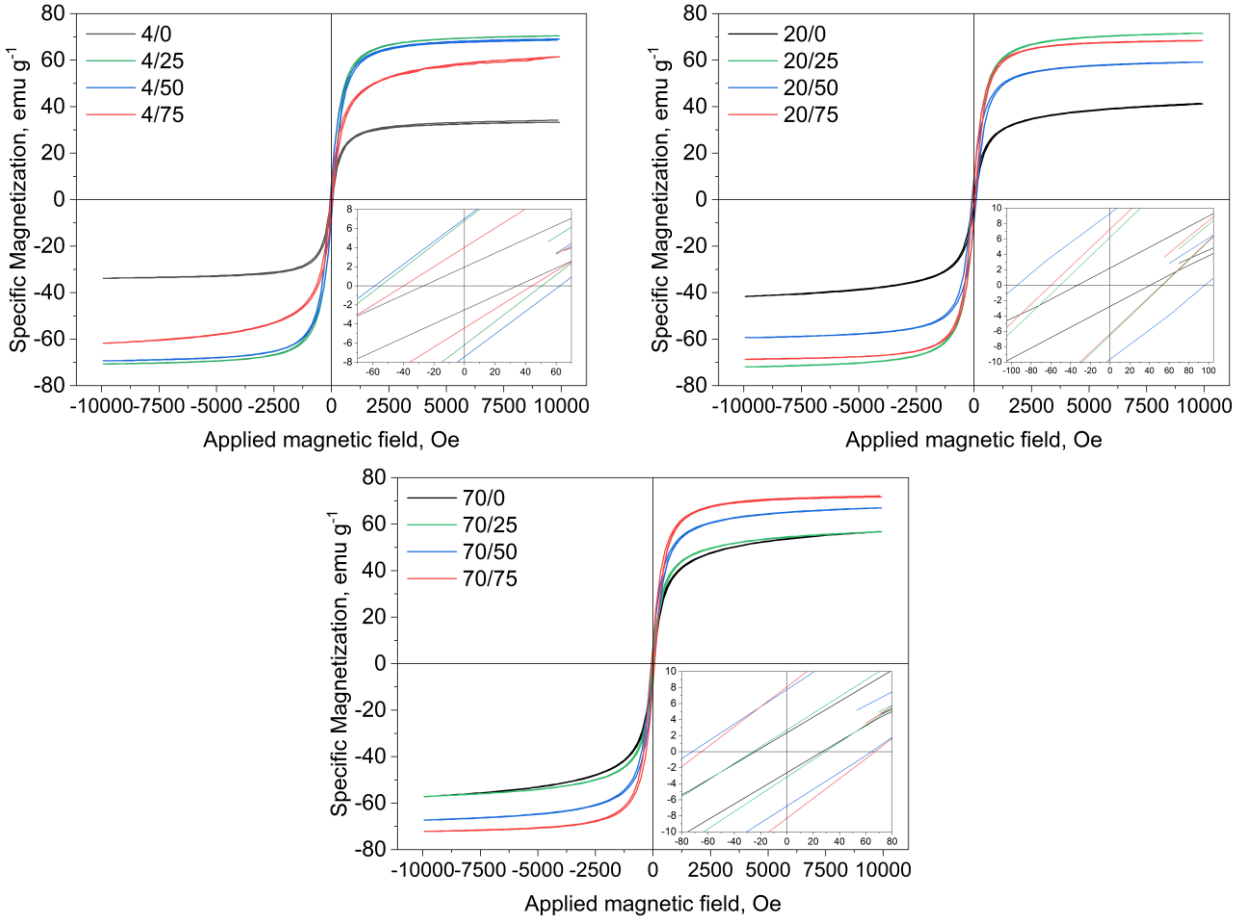

Figure 5. Hysteresis loops of magnetite samples

Table 3

Magnetic characteristics of magnetite samples

Sample	σ_s, emu g^{-1}	σ_r, emu g^{-1}	H_c, Oe
4/0	33.5	2.5	30.0
4/25	70.5	8.0	58.0
4/50	68.7	7.0	55.0
4/75	61.8	4.0	41.0
20/0	41.2	2.5	36.5
20/25	71.9	6.5	45.5
20/50	59.5	9.3	98.0
20/75	68.3	6.7	55.0
70/0	56.7	2.5	25.5
70/25	58.7	2.9	35.5
70/50	67.0	7.7	65.0
70/75	72.0	7.2	70.0

The saturation magnetization (σ_S) of magnetite NPs demonstrates variations influenced synthesis temperature (Fig. 5). Specifically: at a synthesis temperature of 4 °C and 25 % EG content, the saturation magnetization reaches a peak of 70.5 emu g^{-1} before subsequently decreasing. At 20 °C, σ_S does not show a clear correlation with increasing EG content. At 70 °C, σ_S increases from 56.7 to 72 emu g^{-1} as EG content changes. When EG content is 0 % and 75 % in the synthesis solution, σ_S increases from 33.5 and 61.8 emu g^{-1} to 56.7 and 72 emu g^{-1}, respectively. At 25 % EG, σ_S decreases from 70.5 to 56.7 emu g^{-1}, at 50 % EG, σ_S does not exhibit a clear dependence on increasing synthesis temperature (Fig. 6).

The samples exhibiting the highest σ_S values are those synthesized at 20 °C with 25 EG (20/25) and at 70 °C with 75 % EG (70/75).

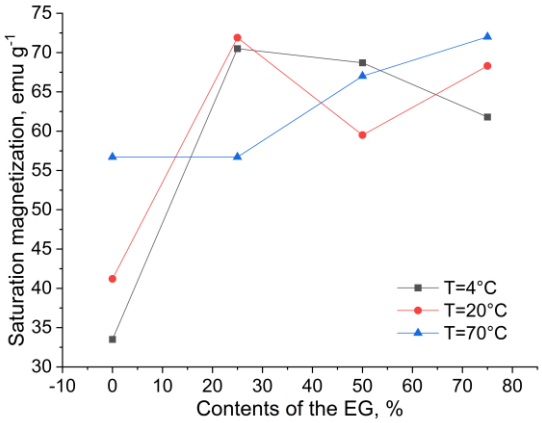

Figure 6. Dependence of saturation magnetization on the EG content in the synthesis solution

As a result, the key factors determining the magnetic characteristics of the synthesized NPs were identified as follows: 1) crystallite size: larger NPs have a smaller specific surface area, which reduces the proportion of disordered spins in the surface layer and leads to an increase in the total magnetic moment; 2) magnetite stoichiometry ($Fe_{3-\delta}O_4$): the saturation magnetization of magnetite directly depends on maintaining the balance between Fe^{2+} and Fe^{3+} ions in the octahedral positions of the crystal lattice, since their electron exchange ensures ferrimagnetic order.

Optimal conditions for synthesizing magnetite NPs with high Fe^{2+} content (Fig. 4*b*) and saturation magnetization (Fig. 6), suitable for ferroptosis-inducing applications were determined to be 25 % EG at 4 °C and 25 °C, and 50 % EG at 70 °C.

Changes in the Viscosity of Nanofluids at NPs Different Concentrations in Polyglucinum

To investigate the influence of NPs on viscosity, samples synthesized at 70 °C were selected. TEM data revealed a linear increase in NPs size from 10 to 34 nm with increasing EG concentration. The intrinsic dynamic viscosity of the PG base fluid, measured at room temperature, was 3.952 mPa s. Figure 7 presents the dynamic viscosity values of PG suspensions containing varying volumes and average particle sizes of Fe_3O_4 NPs with different PDI.

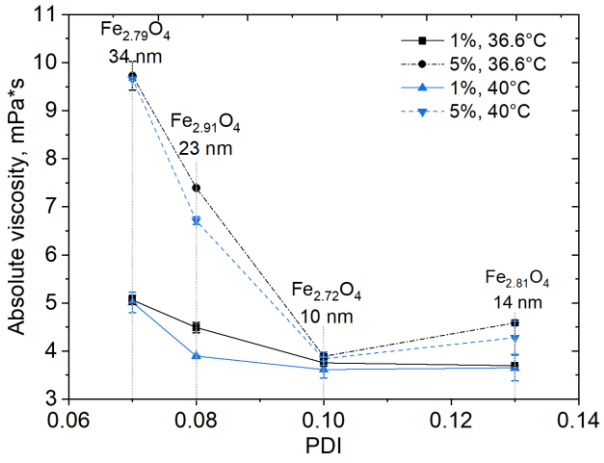

Figure 7. Influence of volume concentration, size and dispersion on the absolute viscosity in Fe_3O_4-PG suspensions (EG/water ratios, vol.%: 70/0, 70/25, 70/50, 70/75)

As shown in Figure 7, the volume concentration of NPs in the PG suspensions ranged from 1 % to 5 %. An increase in NPs content was observed to correlate with an increase in viscosity. At a constant particle size, increasing the NPs concentration causes the flow behavior to transition from Newtonian to shear-

thinning, and subsequently to shear-thickening. In Newtonian regime, low NPs interaction predominates. Shear-thinning arises as weak particle interactions are disrupted at higher shift deformations. At higher particle concentrations, physical collisions and aggregation lead to shear-thickening behavior.

The nanofluid's viscosity increased with larger NPs sizes and decreasing polydispersity index (from 0.13 to 0.07). This is due to the fact that NPs with a wider size span (PDI = 0.13) pack more efficiently than monodisperse particles (PDI = 0.07), creating more free space for NPs movement. Consequently, the fluid flows more easily, resulting in lower viscosity.

Model Experiments: Influence of Magnet Induction on NPs Capture in a Flow-Through Setup

The NPs test sample was synthesized via coprecipitation with EG/water volume ratio of 70/50. This sample exhibited minimal viscosity change in PG, a monodisperse particle size distribution (PDI = 0.08), and high stoichiometry (3–δ = 2.91). These characteristics are crucial for the efficient occurrence of Fenton and Fenton-like processes.

An experimental setup was assembled, considering both hydrodynamic and magnetic parameters (Fig. S2). The setup parameters included: distance from the magnet (0; 0.5; 1; 2; 3; 5 cm); a flow velocity of 9.5 mm s^{-1} (appr. 56.61 cm min^{-1}); introduced NPs masses (0.02, 0.04, 0.08, 0.1, 0.2, 0.3, 0.5 g), and a Neodymium disk magnet (50×20 mm, NbFeB, N42, 298 g) with axial magnetization. The conversion of the distance (*r*) from the magnetite surface to the NPs localization site into magnetic field induction (B) is detailed in SI. Experiments were conducted at room temperature using distilled water as the liquid medium. Gravimetric data analysis, aimed at determining the optimal fixed mass of magnetite NPs on a magnet based on external magnetic field induction, is presented in Table S3 and Figure S4. A mathematical model describing the dependence of NPs capture efficiency on magnetic field parameters and target distance is proposed in Table S4.

A sigmoidal relationship (R^2 = 0.97) was established between the NPs capture efficiency and the magnetic induction (based on the gradient of distance from the target) (Fig. 8). The injection mass at which the proportion of captured NPs reaches its maximum corresponds to the injection mass that maximizes particle capture efficiency. This is defined as the optimal injection mass for maximum injection efficiency (Fig. S5*b* and Table S5).

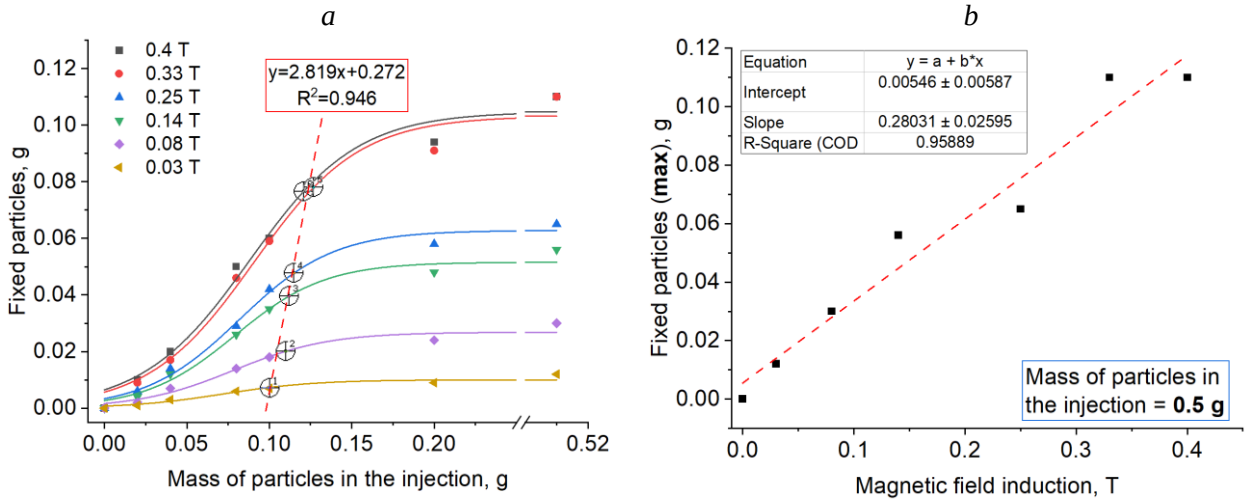

Figure 8. Sigmoid models illustrating the dependence of optimal captured NPs masses (*a*) and the dependence of the saturation mass on magnetic induction (*b*)

Figure 8*a* presents an approximation of the optimal captured NPs masses. Additionally, the maximum capacity line, shown in Figure 8*b*, is significant as it allows for the estimation of the maximum NPs mass reaching the target organ at a given magnetic induction.

Conclusions

In summary, NPs size regulation of Fe_3O_4 can be effectively achieved by adjusting the volume ratio of EG to water. X-ray diffraction data demonstrated that the presence of EG in the reaction mixture, compared to temperature and solution viscosity, is the most significant factor influencing crystallite size. Increasing the

EG concentration to 50 % enhances the Fe_3O_4 stoichiometry, indicating improved oxidation states, while higher concentration beyond this point lead to a decline likely due to restricted hydrolysis pathways that impede Fe_3O_4 NPs formation. Temperature variations influence the magnetite's composition differently depending on EG content with optimal stoichiometry achieved at specific combinations, which correlates directly with saturation magnetization. Additionally, rheological studies with Fe_3O_4-polyglucinum suspensions revealed that viscosity decreases as the particle size distribution broaden from 0.07 to 0.13. This is due to the fact that NPs with a wider size span pack more efficiently than monodisperse particles, creating more free space for NPs movement. Consequently, the fluid flows more easily, resulting in lower viscosity. A mathematical model is proposed to describe the dependence of NPs capture efficiency. A sigmoidal relationship (R^2 = 0.97) was established between the NPs capture efficiency and the magnetic induction gradient. These findings provide insights into controlling NPs synthesis parameters in ambient conditions and suspension properties for advanced magnetic fluid applications.

Supporting Information

The Supporting Information is available free at https://ejc.buketov.edu.kz/ejc/article/view/641/365

Funding

The study was supported by a grant from the Russian Science Foundation (No. 22-73-10222-P, "Preparation, physicochemical characterization and pro-oxidant properties of new iron-containing mesoporous materials", https://rscf.ru/en/project/22-73-10222/).

*Author Information**

**The authors' names are presented in the following order: First Name, Middle Name and Last Name*

Artur Albertovich Dzeranov — Assistant Lecturer, Advanced Materials and Technologies for Aerospace Applications Department, Moscow Aviation Institute (National Research University), Volokolamskoe shosse, 4, 125080, Moscow, Russia; Junior Research Fellow of Laboratory of Metal Polymers, Federal Research Center of Problems of Chemical Physics and Medicinal Chemistry, Russian Academy of Sciences, Semenov avenue, 1, 142432, Chernogolovka, Moscow region, Russia; e-mail: arturdzeranov99@gmail.com; https://orcid.org/0000-0003-3240-9321

Lyubov Sergeevna Bondarenko — PhD (Chemistry), Associate Professor, Advanced Materials and Technologies for Aerospace Applications Department, Moscow Aviation Institute (National Research University), Volokolamskoe shosse, 4, 125080, Moscow, Russia; e-mail: l.s.bondarenko92@gmail.com; https://orcid.org/0000-0002-3107-0648

Michail Vladimirovich Prokofiev — PhD (Chemistry), Associate Professor, Advanced Materials and Technologies for Aerospace Applications Department, Moscow Aviation Institute (National Research University), Volokolamskoe shosse, 4, 125080, Moscow, Russia; e-mail: mikepro1953@rambler.ru

Roman Alexandrovich Bondarenko — PhD Student, Institute of Applied Mechanics of the Russian Academy of Sciences, Leningradsky Prospekt, 7, 125040, Moscow, Russia; e-mail: bondarenko.romaa@yandex.ru; https://orcid.org/0009-0007-8400-5229

Danil Romanovich Abramov — MSc Student, Moscow Aviation Institute (National Research University), Volokolamskoe shosse, 4, 125080, Moscow, Russia; e-mail: dizox13@mail.ru; https://orcid.org/0009-0000-3278-9876

Dzhardimalieva Gulzhian Iskakovna — PhD, DSc (Chemistry), Head of Laboratory of Metallopolymers, Federal Research Center of Problems of Chemical Physics and Medicinal Chemistry, Russian Academy of Sciences, Chernogolovka, Moscow region, 142432, Russia; Professor, Advanced Materials and Technologies for Aerospace Applications Department, Moscow Aviation Institute (National Research University), Volokolamskoe shosse, 4, 125080, Moscow, Russia; e-mail: dzhardim@icp.ac.ru; https://orcid.org/0000-0002-4727-8910

Kamila Asylbekovna Kydralieva — PhD, DSc (Chemistry), Professor, Advanced Materials and Technologies for Aerospace Applications Department, Moscow Aviation Institute (National Research Uni-

versity), Volokolamskoe shosse, 4, 125080, Moscow, Russia; e-mail: kamila.kydralieva@gmail.com; https://orcid.org/0000-0002-4596-4140

Author Contributions

The manuscript was written through contributions of all authors. All authors have given approval to the final version of the manuscript. CRediT: **Artur Albertovich Dzeranov** investigation, writing, editing; **Lyubov Sergeevna Bondarenko** writing, Software; **Michail Vladimirovich Prokofiev** investigation; **Roman Alexandrovich Bondarenko** investigation; **Danil Romanovich Abramov** investigation; **Dzhardimalieva Gulzhian Iskakovna** data curation, conceptualization; **Kamila Asylbekovna Kydralieva** conceptualization, data curation, methodology, writing — reviewing and editing.

Acknowledgments

Magnetic measurements were performed in accordance with the state research assignments registered under No. 124013000757-0. These experiments were carried out using the facilities of *the Multi-User Analytical Center of the Federal Research Center of Problems of Chemical Physics and Medicinal Chemistry of the Russian Academy of Sciences*.

Conflicts of Interest

The authors declare no conflicts of interest.

References

1 Tian, Y., Yu, B., Li, X., & Li, K. (2011). Facile solvothermal synthesis of monodisperse Fe3O4 nanocrystals with precise size control of one nanometre as potential MRI contrast agents. *Journal of Materials Chemistry*, *21*(8), 2476–2481. https://doi.org/10.1039/C0JM02913K

2 Turrina, C., Oppelt, A., Mitzkus, M., Berensmeier, S., & Schwaminger, S. P. (2022). Silica-coated superparamagnetic iron oxide nanoparticles: New insights into the influence of coating thickness on the particle properties and lasioglossin binding. *MRS Communications*, *12*(5), 632–639. https://doi.org/10.1557/s43579-022-00228-y

3 Ulbrich, K., Hola, K., Subr, V., Bakandritsos, A., Tucek, J., & Zboril, R. (2016). Targeted drug delivery with polymers and magnetic nanoparticles: covalent and noncovalent approaches, release control, and clinical studies. *Chemical reviews*, *116*(9), 5338–5431. https://doi.org/10.1021/acs.chemrev.5b00589

4 Reindl, M., Zach, V., & Schwaminger, S. P. (2025). Biocompatible Poly(acrylic acid-co-methacrylic acid)-Coated Iron Oxide Nanoparticles for Enhanced Adsorption and Antimicrobial Activity of Lasioglossin-III. *ACS Applied Materials & Interfaces*, *17*(11), 16644-16657. https://doi.org/10.1021/acsami.4c22603

5 Eigenfeld, M., Reindl, M., Sun, X., & Schwaminger, S. P. (2024). Exploring Multi-Parameter Effects on Iron Oxide Nanoparticle Synthesis by SAXS Analysis. *Crystals*, *14*(11), 961. https://doi.org/10.3390/cryst14110961

6 Pham, A. L. T., Lee, C., Doyle, F. M., & Sedlak, D. L. (2009). A silica-supported iron oxide catalyst capable of activating hydrogen peroxide at neutral pH values. *Environmental science & technology*, *43*(23), 8930–8935. https://doi.org/10.1021/es902296k

7 Saman, D., Bondarenko, L. S., Baimuratova, R. K., Dzeranov, A. A., Dzhardimalieva, G. I., Tropskaya, N. S., & Kydralieva, K. A. (2024). A Statistical Design Approach for an Effective Catalyst in the Fenton Reaction in Case of Fe_3O_4-MOF MIL-88b (Fe) in Methylene Blue Degradation Kinetics. *Eurasian Journal of Chemistry*, *29*(115), 16–29. https://doi.org/10.31489/2959-0663/3-24-15

8 Dzeranov, A., Pankratov, D., Bondarenko, L., Telegina, L., Dzhardimalieva, G., Saman, D., & Kydralieva, K. (2024). Humic acids-modified mesoporous silica encapsulating magnetite: crystal and surface characteristics. *CrystEngComm*, *26*(24), 3250–3262. https://doi.org/10.1039/D4CE00281D

9 Bondarenko, L., Baimuratova, R., Dzeranov, A., Pankratov, D., Kicheeva, A., Sushko, E., ... & Kydralieva, K. (2024). Fenton reaction-driven pro-oxidant synergy of ascorbic acid and iron oxide nanoparticles in MIL-88B (Fe). *New Journal of Chemistry*, *48*(22), 10142–10160. https://doi.org/10.1039/D4NJ00963K

10 Bondarenko, L., Baimuratova, R., Reindl, M., Zach, V., Dzeranov, A., Pankratov, D., ... & Schwaminger, S. P. (2024). Designed magnetic nanoparticles for ferroptosis: Release of iron ions from metal-organic frameworks modified with iron oxides. *Materials Today Chemistry*, *42*, 102332. https://doi.org/10.1016/j.mtchem.2024.102332

11 Dzeranov, A., Bondarenko, L., Pankratov, D., Prokof'ev, M., Dzhardimalieva, G., Jorobekova, S., ... & Kydralieva, K. (2022). Iron oxides nanoparticles as components of ferroptosis-inducing systems: screening of potential candidates. *Magnetochemistry*, *9*(1), 3. https://doi.org/10.3390/magnetochemistry9010003

12 Sahoo, Y., Goodarzi, A., Swihart, M. T., Ohulchanskyy, T. Y., Kaur, N., Furlani, E. P., & Prasad, P. N. (2005). Aqueous ferrofluid of magnetite nanoparticles: fluorescence labeling and magnetophoretic control. *The Journal of Physical Chemistry B*, *109*(9), 3879–3885. https://doi.org/10.1021/jp045402y

13 Lee, N. & Hyeon, T. (2012). Designed synthesis of uniformly sized iron oxide nanoparticles for efficient magnetic resonance imaging contrast agents. *Chemical Society Reviews*, *41*(7), 2575–2589. https://doi.org/10.1039/C1CS15248C

14 Jurgons, R., Seliger, C., Hilpert, A., Trahms, L., Odenbach, S., & Alexiou, C. (2006). Drug loaded magnetic nanoparticles for cancer therapy. *Journal of Physics: Condensed Matter*, *18*(38), S2893. https://doi.org/10.1088/0953-8984/18/38/S24

15 Pankhurst, Q. A., Connolly, J., Jones, S. K., & Dobson, J. J. J. (2003). Applications of magnetic nanoparticles in biomedicine. *Journal of physics D: Applied physics*, *36*(13), R167. https://doi.org/10.1088/0022-3727/36/13/201

16 Laurent, S., Forge, D., Port, M., Roch, A., Robic, C., Vander Elst, L., & Muller, R. N. (2008). Magnetic iron oxide nanoparticles: synthesis, stabilization, vectorization, physicochemical characterizations, and biological applications. *Chemical reviews*, *108*(6), 2064–2110. https://doi.org/10.1021/cr068445e

17 Spicher, M. T., Schwaminger, S. P., Von Der Haar-Leistl, D., Peralta, M. M., Mikacevic, G., Wagner, F. E., & Berensmeier, S. (2024). Pilot-scale co-precipitation synthesis of a novel active ingredient made of ultrasmall iron (oxyhydr) oxide nanoparticles for the treatment of hyperphosphatemia. *RSC advances*, *14*(23), 16117–16127. https://doi.org/10.1039/D4RA02719A

18 Qiao, L., Fu, Z., Li, J., Ghosen, J., Zeng, M., Stebbins, J., ... & Swihart, M. T. (2017). Standardizing size-and shape-controlled synthesis of monodisperse magnetite (Fe_3O_4) nanocrystals by identifying and exploiting effects of organic impurities. *ACS nano*, *11*(6), 6370–6381. https://doi.org/10.1021/acsnano.7b02752

19 Mathew, D. S. & Juang, R. S. (2007). An overview of the structure and magnetism of spinel ferrite nanoparticles and their synthesis in microemulsions. *Chemical engineering journal*, *129*(1–3), 51–65. https://doi.org/10.1016/j.cej.2006.11.001

20 Lu, A. H., Salabas, E. E., & Schüth, F. (2007). Magnetic nanoparticles: synthesis, protection, functionalization, and application. *Angewandte Chemie International Edition*, *46*(8), 1222–1244. https://doi.org/10.1002/anie.200602866

21 Peng, S., & Sun, S. (2007). Synthesis and characterization of monodisperse hollow Fe_3O_4 nanoparticles. *Angewandte Chemie International Edition*, *46*(22), 4155–4158. https://doi.org/10.1002/anie.200700677

22 Schwaminger, S. P., Syhr, C., & Berensmeier, S. (2020). Controlled synthesis of magnetic iron oxide nanoparticles: magnetite or maghemite? *Crystals*, *10*(3), 214. https://doi.org/10.3390/cryst10030214

23 Reindl, M., Zach, V., Cvirn, G., & Schwaminger, S. P. (2025). Influence of coprecipitation synthesis parameters on the physicochemical properties and biological effects of iron oxide nanoparticles. *Nanoscale Advances*, *7*(22), 7395–7407. https://doi.org/10.1039/d5na00632e

24 Schwaminger, S. P., Bauer, D., Fraga-García, P., Wagner, F. E., & Berensmeier, S. (2017). Oxidation of magnetite nanoparticles NanoNPs: impact on surface and crystal properties. *CrystEngComm*, *19*(2), 246–255. https://doi.org/10.1039/C6CE02421A

25 Siregar, N., Indrayana, I. P. T., Suharyadi, E., Kato, T., & Iwata, S. (2017). Effect of synthesis temperature and NaOH concentration on microstructural and magnetic properties of $Mn_{0.5}Zn_{0.5}Fe_2O_4$ nanoparticles. In *IOP Conference Series: Materials Science and Engineering*, *202*(1), 012048. https://doi.org/10.1088/1757-899X/202/1/012048

26 Ghazanfari, M. R., Kashefi, M., & Jaafari, M. R. (2016). Optimizing and modeling of effective parameters on the structural and magnetic properties of Fe_3O_4 nanoparticles synthesized by coprecipitation technique using response surface methodology. *Journal of Magnetism and Magnetic Materials*, *409*, 134–142. https://doi.org/10.1016/j.jmmm.2016.02.094

27 Valenzuela, R., Fuentes, M. C., Parra, C., Baeza, J., Duran, N., Sharma, S. K., ... & Freer, J. (2009). Influence of stirring velocity on the synthesis of magnetite nanoparticles (Fe_3O_4) by the co-precipitation method. *Journal of Alloys and Compounds*, *488*(1), 227–231. https://doi.org/10.1016/j.jallcom.2009.08.087

28 Huang, Z., Tang, F., & Zhang, L. (2005). Morphology control and texture of Fe_3O_4 nanoparticle-coated polystyrene microspheres by ethylene glycol in forced hydrolysis reaction. *Thin Solid Films*, *471*(1-2), 105–112. https://doi.org/10.1016/j.tsf.2004.04.042

29 Furusawa, K., Norde, W., & Lyklema, J. (1972). A method for preparing surfactant-free polystyrene latices of high surface charge. *Kolloid-Zeitschrift & Zeitschrift für Polymere*, *250*(9), 908–909. https://doi.org/10.1007/BF01506246

30 Sobenin, D.V., Solovov, R.D., & Ershov B.G. (2026). Transformation of zerovalent iron nanoparticles in isopropanol into oxide particles: effect of water and air on mechanism and kinetics. *Journal of Molecular Liquids*, *447*, 129333. https://doi.org/10.1016/j.molliq.2026.129333

31 Elmore, W.C. (1938). Ferromagnetic colloid for studying magnetic structures. *Physical Review*, *54*(4), 309–310. https://doi.org/10.1103/PhysRev.54.309

32 Xu, N., Yan, H., Jiao, X., Jiang, L., Zhang, R., Wang, J., Liu, Z., Liu, Z., Gu, Y., Gang, F., Wang, X., Zhao, L., & Sun, X. (2020). Effect of OH^- concentration on Fe_3O_4 nanoparticle morphologies supported by first principle calculation. *Journal of Crystal Growth*, *547*, 125780. https://doi.org/10.1016/j.jcrysgro.2020.125780

33 Bhagwat, S., Singh, H., Athawale, A., Hannoyer, B., Jouen, S., Lefez, B., Kundaliya, D., Pasricha, R., Kulkarni, S., & Ogale, S. (2007). Low temperature synthesis of magnetite and maghemite nanoparticles. *Journal of Nanoscience and Nanotechnology*, *7*(12), 4294–4302. https://doi.org/10.1166/jnn.2007.873

34 Vinila, V.S. & Isac, J. (2022). Chapter 14 — Synthesis and structural studies of superconducting perovskite $GdBa_2Ca_3Cu_4O_{10.5+\delta}$ nanosystems. *Design, Fabrication, and Characterization of Multifunctional Nanomaterials*, 319–341. https://doi.org/10.1016/B978-0-12-820558-7.00022-4

35 Frison, R., Cernuto, G., Cervellino, A., Zaharko, O., Colonna, G. M., Guagliardi, A., & Masciocchi, N. (2013). Magnetite–Maghemite Nanoparticles in the 5–15 Nm Range: Correlating the Core–Shell Composition and the Surface Structure to the Magnetic Properties. A Total Scattering Study. *Chemistry of Materials*, *25*(23), 4820–4827. https://doi.org/10.1021/cm403360f.

36 Dzeranov, A., Bondarenko, L., Saman, D., Prokof'ev, M., Terekhova, V., Telegina, L., Dzhardimalieva, G., Bolotskaya, S., & Kydralieva, K. (2024). Effects of water-induced aging on iron (oxyhydr)oxides nanoparticles: linking crystal structure, iron ion release, and toxicity. *Chemical Papers*. https://doi.org/10.1007/s11696-024-03373-x.

37 Bondarenko, L., Kahru, A., Terekhova, V., Dzhardimalieva, G., Uchanov, P., & Kydralieva, K. (2020). Effects of Humic Acids on the Ecotoxicity of Fe_3O_4 Nanoparticles and Fe-Ions: Impact of Oxidation and Aging. *Nanomaterials*, *10*(10), 2011. https://doi.org/10.3390/nano10102011

38 Chen, L., Ma, J., Li, X., Zhang, J., Fang, J., Guan, Y., & Xie, P. (2011). Strong enhancement on fenton oxidation by addition of hydroxylamine to accelerate the ferric and ferrous iron cycles. *Environmental science & technology*, *45*(9), 3925–3930. https://doi.org/10.1021/es2002748